

Original Paper

# Glycolaldehyde-Derived High-Molecular-Weight Advanced Glycation End-Products Induce Cardiac Dysfunction through Structural and Functional Remodeling of Cardiomyocytes

Dorien Deluyker<sup>a</sup> Lize Evens<sup>a</sup> Sibren Haesen<sup>a</sup> Ronald B. Driesen<sup>a</sup>  
Diederik Kuster<sup>b</sup> Maxim Verboven<sup>a</sup> Hanne Belien<sup>a</sup>  
Jolanda van der Velden<sup>b</sup> Ivo Lambrichts<sup>a</sup> Virginie Bito<sup>a</sup>

<sup>a</sup>Biomedical Research Institute, Hasselt University, Hasselt, Belgium, <sup>b</sup>Amsterdam UMC, Vrije Universiteit Amsterdam, Physiology, Amsterdam Cardiovascular Sciences, Amsterdam, The Netherlands

## Key Words

High-molecular-weight advanced glycation end-products • AGEs • Adult rat cardiomyocytes • Electrophysiology • Electron microscopy • Mitochondria

## Abstract

**Background/Aims:** High-molecular-weight advanced glycation end-products (HMW-AGEs) are abundantly present in our Western diet. There is growing evidence reporting that HMW-AGEs contribute to the development of cardiovascular dysfunction *in vivo*, next to the well-known low-molecular-weight AGEs. The goal of our study is to assess the ultrastructure and function of cardiomyocytes after chronic exposure to HMW-AGEs. A better understanding of underlying mechanisms is essential to create new opportunities for further research on the specific role of HMW-AGEs in the development and progression of cardiovascular diseases. **Methods:** Adult male rats were randomly assigned to daily intraperitoneal injection for six weeks with either HMW-AGEs (20 mg/kg/day) or a control solution. Hemodynamic measurements were performed at sacrifice. Single cardiomyocytes from the left ventricle were obtained by enzymatic dissociation through retrograde perfusion of the aorta. Unloaded cell shortening, time to peak and time to 50% relaxation were measured during field stimulation and normalized to diastolic length. L-type Ca<sup>2+</sup> current density ( $I_{CaL}$ ) and steady-state inactivation of  $I_{CaL}$  were measured during whole-cell ruptured patch clamp. Myofilament functional properties were measured in membrane-permeabilized cardiomyocytes. Ultrastructural examination of cardiac tissue was performed using electron microscopy. **Results:** Rats injected with HMW-AGEs displayed *in vivo* cardiac dysfunction, characterized by significant changes in

D. Deluyker and L. Evens contributed equally to this work.

left ventricular peak rate pressure rise and decline accompanied with an increased heart mass. Single cardiomyocytes isolated from the left ventricle revealed concentric hypertrophy, indicated by the increase in cellular width. Unloaded fractional cell shortening was significantly reduced in cells derived from the HMW-AGEs group and was associated with slower kinetics. Peak L-type  $\text{Ca}^{2+}$  current density was significantly decreased in the HMW-AGEs group. L-type  $\text{Ca}^{2+}$  channel availability was significantly shifted towards more negative potentials after HMW-AGEs injection. The impact of HMW-AGEs on myofilament function was measured in membrane-permeabilized cardiomyocytes showing a reduction in passive force, maximal  $\text{Ca}^{2+}$  activated force and rate of force development. Ultrastructural examination of cardiac tissue demonstrated adverse structural remodeling in HMW-AGEs group characterized by a disruption of the cyto-architecture, a decreased mitochondrial density and altered mitochondrial function. **Conclusion:** Our data indicate that HMW-AGEs induce structural and functional cellular remodeling via a different working mechanism as the well-known LMW-AGEs. Results of our research open the door for new strategies targeting HMW-AGEs to improve cardiac outcome.

© 2020 The Author(s). Published by  
Cell Physiol Biochem Press GmbH&Co. KG

## Introduction

Cardiovascular diseases (CVDs) are common health problems experienced by our aging Western population. These pathologies have a high probability to progress into end-stage heart failure (HF) which is defined as the inability of the heart to pump enough blood and meet the energy demand of the body [1, 2]. The development of HF is a complex process involving a series of physiological and molecular factors and is characterized by structural and functional disorders that remain incompletely understood. Advanced glycation end-products (AGEs) are important components of our Western diet as described previously by our group [3], and are thought to contribute to the development and progression of CVDs [4]. AGEs are a collective term for the heterogeneous group of compounds formed by irreversible glycation of proteins [5, 6]. AGEs are known to affect cellular function by two mechanisms: (a) cross-linking intracellular (*e.g.* sarco/endoplasmic reticulum  $\text{Ca}^{2+}$  ATPase (SERCA)) or extracellular proteins (*e.g.* collagen) or (b) activating intracellular cascades after binding to their receptor RAGE [7, 8]. AGEs can be distinguished by their different mechanisms of action and/or fluorescent properties. Besides, AGEs can also be classified into low-molecular-weight AGEs (LMW-AGEs, <12 kDa) and high-molecular-weight AGEs (HMW-AGEs, >12 kDa). LMW-AGEs circulate as free proteins while HMW-AGEs are considered to be protein-bound compounds [9, 10]. Over the past few years, evidence is growing that AGEs contribute to the development and progression of cardiovascular dysfunction [11, 12]. While most of these studies focus primarily on LMW-AGEs, very little is reported on HMW-AGEs. However, their importance in cardiac pathophysiology is rising [13, 14]. We have previously shown that HMW-AGEs are responsible for cardiac dysfunction (*i.e.* myocardial hypertrophy and fibrosis) in healthy rats, independent of RAGE activation [15]. Whether the cardiac dysfunction seen *in vivo* is the result of profound remodeling at the cellular level remains unknown and this study aims to investigate this. We hypothesize that chronic exposure of HMW-AGEs will promote maladaptive remodeling of adult cardiomyocytes through alteration of their contractile properties and induction of ultrastructural abnormalities.

## Materials and Methods

### *Animal model*

Adult male Sprague Dawley rats (Charles River Laboratories, Lyon, France) were used. The animals were daily injected intraperitoneally (*i.p.*) for six weeks with HMW-AGEs (20 mg/kg/day, N=25) or an equal amount of unmodified bovine serum albumin (BSA) as control solution (N=19), as previously described [15]. Briefly, fatty acid-free and low endotoxin bovine serum albumin (BSA; 7 mg/ml) was incubated with

90 mM glycolaldehyde dimers (Sigma-Aldrich, Diegem, Belgium) in phosphate buffered saline (PBS) (pH 7.4) for 5 days at 37°C (BSA-derived AGEs). A control sample was prepared in parallel by incubation of BSA (7 mg/ml) in PBS. Unreacted glycolaldehyde was removed by dialysis against PBS using a cut-off value of 3.5 kDa and filter sterilized (0.2 µm sterile filter, Sarstedt, Essen, Belgium). Finally, the samples were concentrated using Amicon Ultra Centrifugal Filter Units with Ultracel-50 membrane (Millipore, Brussel, Belgium). All animals were maintained in a controlled environmental condition of temperature and humidity, were fed a standard pellet diet and had water available *ad libitum*. After six weeks of daily injections, conventional echocardiographic images were obtained in rats anesthetized via inhalation with 3% isoflurane supplemented with oxygen as described previously [16] and invasive hemodynamic measurements were performed. Finally, the heart was harvested and left ventricular (LV) single cardiomyocytes were isolated, as previously described [14]. Tissue of both animal groups was fixed overnight with 2% glutaraldehyde in 0.05 M cacodylate buffer at 4°C for light microscopic (LM) and electron microscopic (EM) examination or were fixed overnight in 4% paraformaldehyde and transferred in 70% ethanol until embedded in paraffin. Subsequently, 8 µm thick sections were cut and stored at room temperature until staining.

### *Hemodynamic measurements*

Just before sacrifice, hemodynamic measurements were conducted in rats anesthetized via inhalation with 3% isoflurane supplemented with oxygen. Functional cardiac parameters were measured in the LV via the right carotid artery, as described previously [3, 16]. Heart rate (HR), maximum and minimum peak time derivatives ( $dP/dt_{\max}$  and  $dP/dt_{\min}$  respectively) and time constant for isovolumetric relaxation (Tau) were measured with the SPR 320 Rat Pressure Catheter (AD Instruments, Germany) for 10 minutes to ensure stable recordings. The data were analyzed with LabChart 7 software (AD instruments, United Kingdom).

### *Cardiomyocyte isolation*

After six weeks of treatment, rats were injected with heparin (1000 u/kg *i.p.*) and sacrificed with an overdose of pentobarbital (150 mg/kg *i.p.*). Hearts were dissected and weighted. Single adult cardiomyocytes from the LV were obtained by enzymatic dissociation through retrograde perfusion of the aorta, as previously described [14]. The hearts were perfused with normal Tyrode (NT) (in mM, NaCl 137, KCl 5.4, MgCl<sub>2</sub> 0.5, CaCl<sub>2</sub> 1, Na-HEPES 11.8, glucose 10 and taurine 20; pH 7.35) on a Langendorff setup at 37°C. After perfusion with a Ca<sup>2+</sup>-free solution (in mM: NaCl 130, KCl 5.4, KH<sub>2</sub>PO<sub>4</sub> 1.2, MgSO<sub>4</sub> 1.2, HEPES 6, glucose 20; pH 7.2), the tissue was perfused with an enzyme solution (Ca<sup>2+</sup>-free solution supplemented with collagenase type II (1.5 g/l; Worthington, Lakewood, USA) and protease type XIV (0.06 g/l; Sigma, Diegem, Belgium)), followed by a low-Ca<sup>2+</sup> solution (NT with 0.1 mM CaCl<sub>2</sub>). The digested LV tissue was minced and subsequently filtered with a mesh of 300 µm. A part of the freshly isolated cells was used to assess unloaded cell shortening or perform electrophysiology measurements. Experiments were performed at room temperature within six hours after cell isolation. The remaining cells were stored at -80 °C and used for protein expression analysis and experiments on myofilament function.

### *Cell size and unloaded cell shortening measurements*

Isolated cardiomyocytes were placed into a perfusion chamber with NT, on the stage of an inverted microscope (Nikon Diaphot, Groot-Bijgaarden, Belgium). Cardiomyocyte length and width were measured in ± 25 cells per animal. Unloaded cell shortening of intact cardiomyocytes was measured with a video-edge detector (Crescent Electronics, London, UK). Field stimulation was done with pulses of constant voltage using platinum electrodes. Steady-state stimuli were applied at frequencies of 1, 2 and 4 Hz. Unloaded cell shortening was normalized to diastolic cell length ( $L/L_0$ ). Time to peak contraction (TTP) and time to half-maximal relaxation ( $RT_{50}$ ) were measured to assess kinetics of cell shortening. Unloaded fractional cell shortening was also measured at 1 Hz before and after adding isoproterenol (ISO; 300 nM).

### *Electrophysiology measurements*

L-type Ca<sup>2+</sup> current ( $I_{\text{cal}}$ ) was measured during whole-cell voltage-clamp and was normalized to cell capacitance, a measure of cell surface. Patch pipettes (resistance: 2-3 MΩ) were filled with a pipette solution (in mM: KAsp 120, KCl 20, HEPES 10, MgATP 5, EGTA 10, NaCl 10; pH 7.2).  $I_{\text{cal}}$  was measured by a single depolarizing step of 150 ms from -40 mV to +10 mV. The voltage inactivation component was derived by using biexponential fitting of  $I_{\text{cal}}$  inactivation obtained during the single depolarizing step to +10 mV. The

full current-voltage relationship of  $I_{CaL}$  was measured during 10 mV depolarizing steps ranging from -40 mV to +60 mV. Steady-state inactivation and activation were determined with a classical two-steps protocol described previously [17]. In brief, inactivating prepulses of 400 ms were applied from a holding potential of -70 mV to various potentials. Amplitudes of the peak inward current during the test pulse ( $I$ ) at 0 mV were normalized to their respective maximum value ( $I_{max}$ ) and were plotted as a function of the inactivating potential. Values were fitted with the Boltzmann equation:  $I/I_{max} = (1-A)/\{1+\exp [(V-V_{1/2})/k]\}+A$ , where  $V_{1/2}$  is the potential of half-maximal inactivation,  $k$  is the slope factor and  $A$  is the amplitude of the non-inactivating current. A steady-state activation plot was generated by dividing peak  $I_{CaL}$  measured at a given potential by the difference between measured and reversal potential. Amplitudes of the channel conductance during the test pulse ( $G$ ) were normalized to their respective maximum value ( $G_{max}$ ) and were plotted as a function of the activating potential. Values were calculated by:  $I/I_{max} = 1/\{1+\exp [(V_{1/2}-V)/k]\}$ , as described by Vornanen *et al.* [18].

### *Cardiomyocyte skinning and measurements of isometric force*

Single skinned cardiomyocytes were prepared from frozen cell pellets. The pellet was first thawed in a  $Ca^{2+}$ -free relaxing solution (in mM:  $Na_2ATP$  6,  $MgCl_2$  6, EGTA 2, KCl 140, imidazole 10; pH 7.0). Thawed cardiomyocytes were incubated for five minutes in the same solution with 0.5% Triton X-100 to permeabilize and remove lipid membranes. Isometric force was measured in skinned cardiomyocytes fixed between a piezoelectric motor and a force transducer at 15 °C. Absolute forces were normalized to the cross-sectional area of cardiomyocytes and expressed as developed tension. Passive force ( $F_{pass}$ ) was measured at different sarcomere lengths in  $Ca^{2+}$ -containing relaxing solution (in mM:  $Na_2ATP$  5.89,  $MgCl$  6.48, K-propionate 4.76, N,N-Bis(2-hydroxyethyl)-2-aminoethanesulfonic acid (BES) 100,  $Ca^{2+}$ -EGTA 7 and creatine phosphate 14.5; pH 7.0) by slackening the myocyte by 30% of its length [19, 20]. Active tension ( $F_{act}$ ) was calculated as  $F_{act} = F_{total} - F_{pass}$ . After the steady-state force was reached, cardiomyocytes were allowed to shorten to 30% of their original length and were then restretched to the original length. The rate of force redevelopment ( $K_{tr}$ ) was derived from a single exponential fit of force redevelopment.

### *Assessment of cardiomyocyte organization*

In a subset of animals, LV tissue was processed for both LM and EM examination of cardiomyocyte organization. Tissues of both animal groups were fixed overnight with 2% glutaraldehyde in 0.05M cacodylate buffer at 4 °C, post-fixed in 2% osmium tetroxide and stained with 2% uranyl acetate in 10% acetone. Samples were dehydrated in graded series of acetone and embedded in araldite according to the pop-off method. Semi-thin sections were stained with toluidine blue and randomly selected for LM examination. Mitochondrial surface area (deep blue color) was assessed in LM and quantified using the threshold tool in ImageJ [21]. Data were expressed as percentage area occupied by mitochondria relative to total cell area. Subsequently, ultra-thin sections were cut and mounted on formvar-coated grids, counterstained with uranyl acetate and lead citrate, and were imaged in a Philips EM 208 transmission electron microscope (Philips, Eindhoven, Netherlands). Random EM pictures of cardiomyocytes with a visible nucleus were taken at 1800x and 14000x magnification.

Per animal, 5 EM pictures were taken to perform deep morphological analysis of intracellular cardiomyocyte organization. Mitochondrial density was calculated as the number of mitochondria, measured using the cell counter tool in ImageJ, normalized to total cell area. The mitochondrial, myofibrillar, nuclear and cytoplasm surface area were measured by grid-point analysis in ImageJ, counting every point (distance = 2  $\mu$ m) at the intersection of horizontal and vertical lines [21]. Data were presented as percentage of points hitting the different structures relative to total grid points. All samples were coded, and image analysis was performed single blinded.

### *Statistical analysis*

Statistical analysis was performed using GraphPad Prism (GraphPad software, version 7, San Diego, CA, USA). All data are expressed as mean  $\pm$  standard error of the mean (SEM). Normal distribution of data was verified by the Shapiro-Wilk test. Data sets that passed normality were compared with the parametric unpaired t-test, while the non-parametric Mann-Whitney U test was used otherwise. In addition, two-way ANOVA test was used when appropriate followed by Tukey's *post hoc* test. Finally, paired t-test was used for the data before and after application of ISO. A value of  $P < 0.05$  was considered statistically significant.

## Results

### *HMW-AGEs alter global LV function in vivo*

Hemodynamic parameters obtained after six weeks treatment were summarized in Table 1. Maximum peak time of pressure rise ( $dP/dt_{max}$ ), used as a measure of ventricular contractility, was significantly decreased while ventricular relaxation, assessed by minimum peak time of pressure decline ( $dP/dt_{min}$ ) was significantly increased after six weeks of HMW-AGEs injections ( $p < 0.05$ ). Tau remained comparable between groups (Table 1).

### *HMW-AGEs induce morphological remodeling*

As shown in Fig. 1A, heart weight/body weight (HW/BW) and heart weight/tibia length (HW/TL) ratios were significantly increased in HMW-AGEs-treated animals indicating an increased heart mass. This increase was further confirmed by the increased anterior wall thickness (AWT) and posterior wall thickness (PWT) assessed by conventional echocardiographic as previously described by Deluyker *et al.* [15] and reported in Supplementary Table 1. While cell length was not statistically different between groups, cell width was significantly increased in HMW-AGEs-treated animals ( $24 \pm 0.3 \mu\text{m}$  vs  $21.8 \pm 0.4 \mu\text{m}$  in control,  $p < 0.05$ ) (Fig. 1B). As shown in Fig. 1C, cell width distribution was shifted towards higher cell width values in cardiomyocytes from HMW-AGEs injected animals, further confirming an overall increase in cell width in the treated group.

### *HMW-AGEs cause contractile impairment*

A representative example of fractional cell shortening during field stimulation at 1 Hz in both groups is shown in Fig. 2A. As summarized in Fig. 2B, unloaded cell shortening was significantly reduced in HMW-AGEs group. Both TTP and  $RT_{50}$  at 1 Hz were significantly increased in HMW-AGEs group ( $p < 0.05$ ; Fig. 2B). Altogether, these data indicate a reduced contraction associated with slower kinetics. Smaller and slower contractions were also seen at higher frequencies, *i.e.* 2 and 4 Hz (Supplementary Fig. 1). Additionally, unloaded cell shortening was measured before and after application of ISO (Fig. 2C). Adrenergic stimulation increased unloaded cell shortening to the same extent in both groups indicating an unaltered contractile reserve in the treated animals.

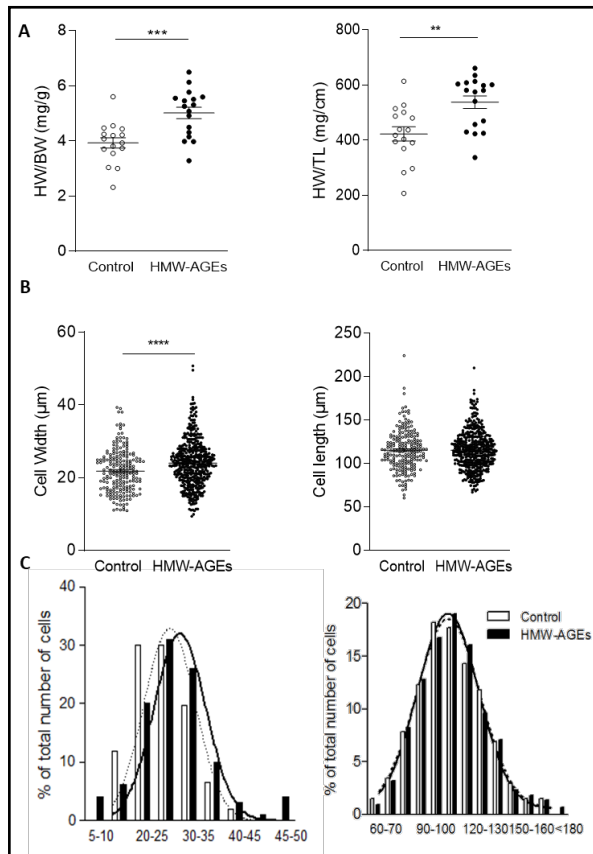
To further unravel the underlying mechanisms resulting in impaired cardiomyocyte relaxation, we examined protein levels of SERCA, PLN and its phosphorylated forms and NCX (data not shown). Protein levels were not different between groups. As shown in Supplementary Fig. 2, the impaired cardiomyocyte relaxation observed after 6 weeks injection of HMW-AGEs was accompanied with a decrease in  $\text{Ca}^{2+}$  ATPase activity ( $p = 0.07$ ). Finally, there was no difference observed in the ratio  $\text{MHC-}\alpha/\text{MHC-}\beta$  between both groups (Supplementary Fig. 3).

To get more insights into the mechanisms resulting in a reduced contractile capacity of single cardiomyocytes, we examined intrinsic properties of myofilaments in skinned myocytes. As shown in Fig. 3A, passive force was significantly reduced in HMW-AGEs group at all sarcomere lengths. Maximal  $\text{Ca}^{2+}$ -activated active force at  $2.2 \mu\text{m}$  sarcomere length tended to be reduced in HMW-AGEs group ( $18 \pm 2 \text{ kN/m}^2$  in control group vs  $13 \pm 1 \text{ kN/m}^2$  in HMW-AGEs group,  $p = 0.06$ , Fig. 3B). Finally, the rate of force redevelopment ( $K_{tr}$ ) was significantly smaller in HMW-AGEs group (Fig. 3C).

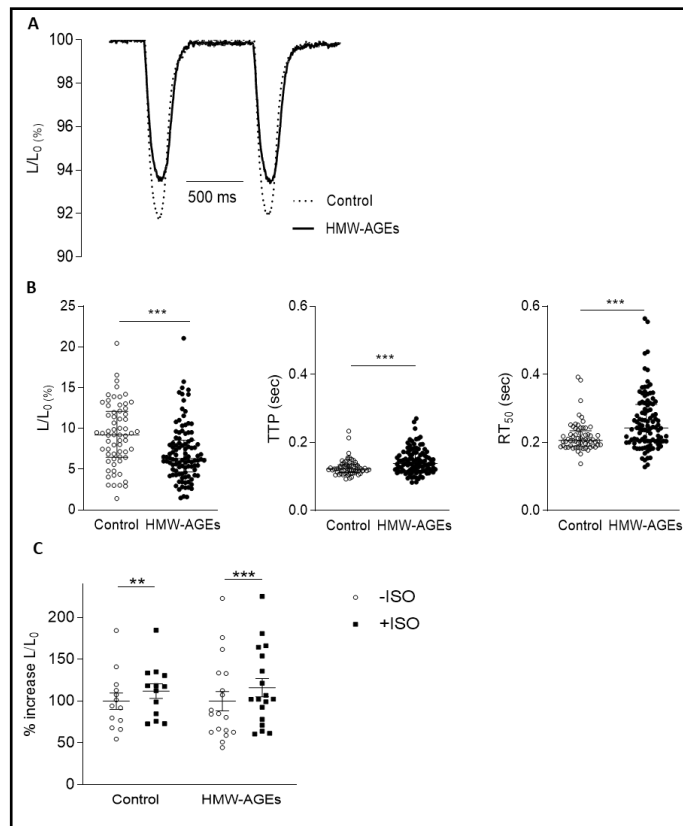
**Table 1.** Hemodynamic parameters after six weeks HMW-AGEs injections. These parameters were evaluated six weeks post-injections in control (N=12) and HMW-AGEs (N=10). Data are presented as mean  $\pm$  SEM. \* denotes  $p < 0.05$ . HR, heart rate; bpm, beats per minute;  $dP/dt_{max}$ , maximum peak time of pressure rise;  $dP/dt_{min}$ , minimum peak time pressure decline; Tau, time constant of LV pressure decay during isovolumetric relaxation period

Parameters	Control	HMW-AGEs
HR (bpm)	367.08 $\pm$ 6.38	363.62 $\pm$ 9.07
$dP/dt_{max}$ (mmHg/s)	7358.10 $\pm$ 405.93	6282.96 $\pm$ 286.02 *
$dP/dt_{min}$ (mmHg/s)	-6387.12 $\pm$ 266.26	-5426.41 $\pm$ 262.89 *
Tau (s)	0.64 $\pm$ 0.015	0.46 $\pm$ 0.015

**Fig. 1.** HMW-AGEs induce hypertrophy. (A) Heart weight/body weight (HW/BW, mg/g,  $p=0.0006$ , parametric unpaired t-test) and HW/tibia length (HW/TL, mg/cm,  $p=0.0021$ , parametric unpaired t-test) in control ( $N=16$ ) and HMW-AGEs ( $N=17$ ) animals. (B) Analysis of cardiomyocyte width ( $\mu\text{m}$ ,  $p<0.0001$ , parametric unpaired t-test) and length ( $\mu\text{m}$ ,  $p=0.9628$ , parametric unpaired t-test) in control ( $n_{\text{cells}}=203$ ) and HMW-AGEs ( $n_{\text{cells}}=436$ ). (C) Frequency distribution of cardiomyocyte width and length in both groups. Data are expressed as mean  $\pm$  SEM. \*\* denotes  $p<0.001$ , \*\*\* denotes  $p<0.0001$ .



**Fig. 2.** HWM-AGEs reduce cellular contractile properties. (A) Representative example of unloaded cell shortening during field stimulation at 1 Hz in control and HMW-AGEs group. (B) Fractional cell shortening normalized to cell length ( $L/L_0$ , %,  $p=0.0001$ , non-parametric Mann-Whitney U test), time to peak of contraction (TTP, sec,  $p=0.0002$ , non-parametric Mann-Whitney U test) and time to half-relaxation (Time to  $RT_{50}$ , sec,  $p=0.0002$ , non-parametric Mann-Whitney U test) in cardiomyocytes derived from control ( $n_{\text{cells}}=64$ ) or HMW-AGEs-treated ( $n_{\text{cells}}=104$ ) animals. Data are expressed as median with interquartile range (C) Relative change in fractional cell shortening normalized to cell length ( $L/L_0$ , %) at 1 Hz before and after isoproterenol (ISO) application in control ( $n_{\text{cells}}=13$ ,  $p<0,01$ , two-way ANOVA) or HMW-AGEs cardiomyocytes ( $n_{\text{cells}}=18$ ,  $P<0.01$ , two-way ANOVA). Data are expressed as mean  $\pm$  SEM. \*\* denotes  $p<0.001$ , \*\*\* denotes  $P<0.0001$ .



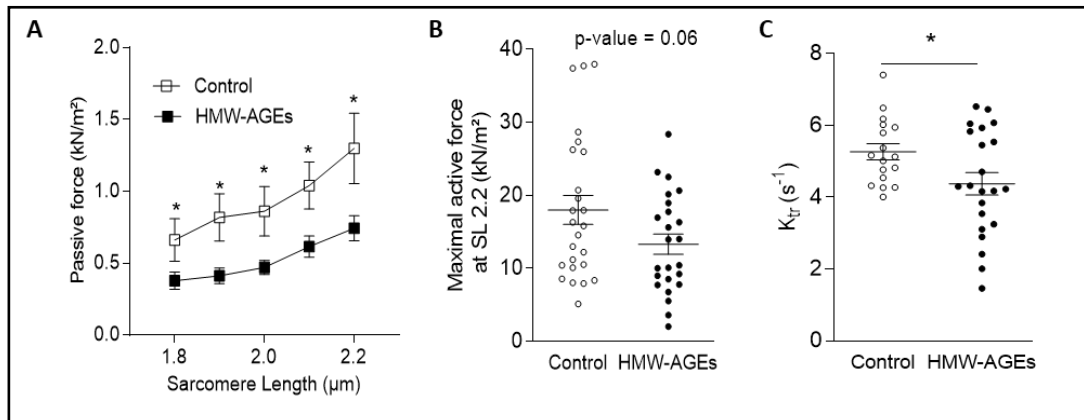


**Fig. 3.** Force development in skinned single myocytes is reduced with HMW-AGEs injections. (A) Passive force at different sarcomere lengths (two-way ANOVA followed by Tukey's post hoc test) and (B) active force at sarcomere length 2.2 µm, both normalized to cross-sectional area (kN/m<sup>2</sup>) in control (n<sub>cells</sub>=25) and HMW-AGEs group (n<sub>cells</sub>=24) (p=0.06, parametric unpaired t-test) (C) The rate of force redevelopment (K<sub>tr</sub>, s<sup>-1</sup>, P=0.03, parametric unpaired t-test) in control (n<sub>cells</sub>=17) and HMW-AGEs (n<sub>cells</sub>=22) group. Data are expressed as mean ± SEM. \* denotes P<0.05 vs control.

#### HMW-AGEs alter L-type Ca<sup>2+</sup> channel properties

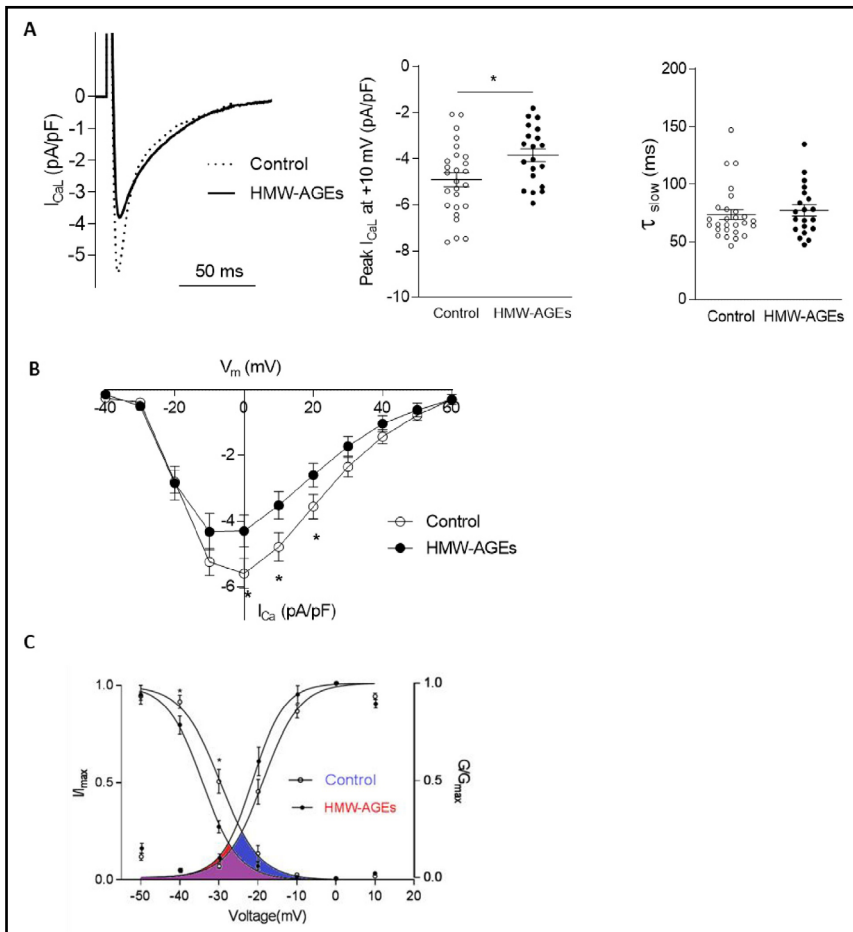
A representative current recording elicited by a depolarizing step from -40 to +10 mV is shown in Fig. 4A, left panel. The associated peak I<sub>CaL</sub> density was significantly smaller in cardiomyocytes derived from HMW-AGEs injected animals (Fig. 4A, mid panel). The slow inactivation component of Ca<sup>2+</sup> current (voltage-dependent, τ<sub>slow</sub>) was not statistically different between groups (Fig. 4A, right panel). As summarized in Fig. 4B, voltage-dependence of I<sub>CaL</sub> remained bell-shaped in HMW-AGEs group. In addition, peak I<sub>CaL</sub> was significantly smaller in HMW-AGEs at depolarizing steps of maximal I<sub>CaL</sub> activation (*i.e.* 0, 10 and 20 mV).

To further investigate potential changes in the intrinsic properties of L-type Ca<sup>2+</sup> channels, steady-state inactivation and steady-state activation of I<sub>CaL</sub> were evaluated (Fig. 4C). As shown in Table 2, HMW-AGEs injections led to a statistically significant shift towards more negative potentials of steady-state inactivation of I<sub>CaL</sub>, a measure of channel availability. Indeed, voltage value at 50% inactivation (V<sub>50</sub>) was at -29.6 ± 0.5 mV in control and -34.2 ± 0.5 mV in HMW-AGEs group, p<0.05 (Table 2). Steady-state activation of I<sub>CaL</sub>, a measure of channel conductance was not significantly different between the groups. As a result, the Ca<sup>2+</sup> window current was smaller in HMW-AGEs group (Fig. 4C).

#### HMW-AGEs cause ultrastructural and functional mitochondrial remodeling in cardiomyocytes

To investigate the impact of HMW-AGEs on cardiomyocyte mitochondria, we quantified the mitochondrial surface area using light-microscopy evaluation of toluidine blue-stained sections (Fig. 5A). This analysis revealed that mitochondrial area was significantly smaller in cardiomyocytes from HMW-AGEs-treated animals compared to non-treated controls (21 ± 0.3% vs 24 ± 0.5% in control animals, p<0.0001; Fig. 5B). Ultrastructural examination using grid-point analysis of electron microscopy (EM) pictures (Fig. 5C) confirmed the reduction in mitochondrial surface area in HMW-AGEs group (Fig. 5D, first panel) (33 ± 0.9% vs 36 ± 1.2% in control animals, p<0.05), further confirming data obtained with light microscopy. To evaluate whether the decrease in mitochondrial surface area was related to a loss in mitochondrial number, we measured the mitochondrial density, *i.e.* mitochondrial number per total cell area. The latter analysis revealed a significantly reduced mitochondrial number per cell area in cardiomyocytes from HMW-AGEs animals (0.40 ± 0.1 vs 0.46 ± 0.1 in control animals, p<0.05; Fig. 5D, second panel). Furthermore, in control condition, analysis of EM pictures revealed a mitochondrial network interspersed between regularly organized myo-

**Fig. 4.** L-type  $\text{Ca}^{2+}$  current density is reduced with HMW-AGEs injections. (A) Representative example of L-type  $\text{Ca}^{2+}$  current ( $I_{\text{CaL}}$ , pA/pF) density elicited by a depolarizing step from -40 mV to +10 mV in control and HMW-AGEs group (left panel). Peak  $I_{\text{CaL}}$  normalized to cell capacitance (pA/pF) in cardiomyocytes derived from control ( $n_{\text{cells}}=26$ ) and HMW-AGEs-injected ( $n_{\text{cells}}=20$ ) animals (mid panel). Data are shown as mean  $\pm$  SEM. \* denotes  $P<0.05$  vs control ( $p=0.016$ , parametric unpaired t-test). Slow time ( $\tau_{\text{slow}}$ , ms) constant in cardiomyocytes from control ( $n_{\text{cells}}=27$ ) and HMW-AGEs ( $n_{\text{cells}}=20$ ) animals (right panel). Data are expressed as mean  $\pm$  SEM ( $p=0.5016$ , parametric unpaired t-test).



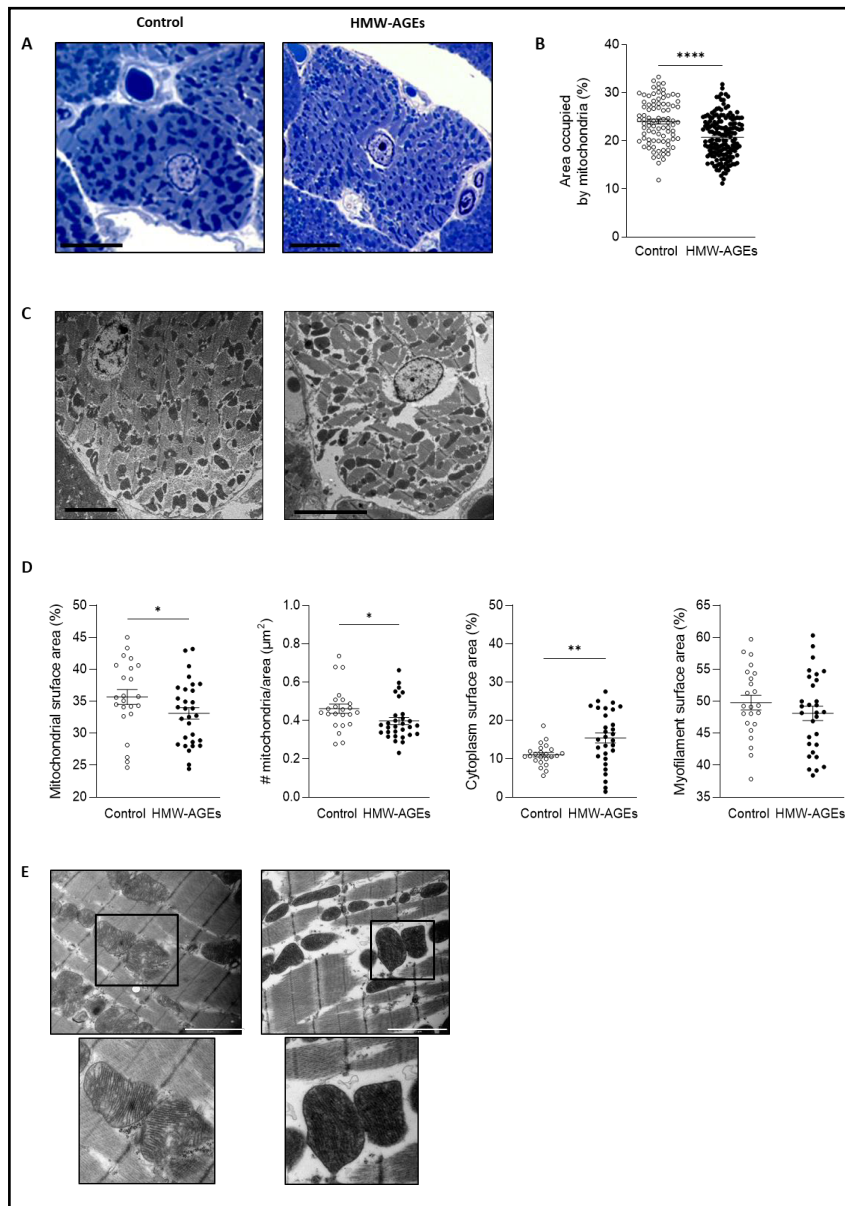
(B) Voltage-dependence of  $I_{\text{CaL}}$  (mV) in cardiomyocytes from control ( $n_{\text{cells}}=18$ ) and HMW-AGEs ( $n_{\text{cells}}=12$ ) animals. Data are expressed as mean  $\pm$  SEM. \* denotes  $p<0.05$  vs control (2-way ANOVA followed by Tukey's post hoc test. (at 0 mV  $p=0.0364$ , at 10 mV  $p=0.0238$ , at 20 mV 0.0438) (C) Steady-state activation and inactivation of  $I_{\text{CaL}}$  in control ( $n_{\text{cells}}=12$ ) cardiomyocytes (blue) and in HMW-AGEs ( $n_{\text{cells}}=8$ ) derived cardiomyocytes (red). Amplitudes of the peak inward current during the test pulse (I) were normalized to their respective maximum value ( $I_{\text{max}}$ ) and are plotted as a function of the inactivating potential. Amplitudes of channel conductance during the test pulse (G) were normalized to their respective maximum value ( $G_{\text{max}}$ ) and are plotted as a function of the activating potential. The activation window is indicated in color; blue for the control animals, red for the animals subjected to HMW-AGEs injection and violet for the overlap between both groups. Data are expressed as mean  $\pm$  SEM. \* denotes  $p<0.05$  vs control.

filaments. However, in the treated group, the loss in mitochondrial content was accompanied by a disarrangement of the mitochondrial network and a statistically significant increase in area occupied by cytoplasm devoid of mitochondria and myofilaments ( $15 \pm 1.3\%$  vs  $11 \pm 0.6\%$  in control animals,  $p<0.01$ ; Fig. 5D, third panel). To determine whether the increase in cytoplasm area was related to a degenerative breakdown of myofilaments, we quantified myofilament surface area using the aforementioned grid-point analysis. This analysis showed no statisti-

**Table 2.** HMW-AGEs alter intrinsic properties of the L-type  $\text{Ca}^{2+}$  channel. Voltage value at 50% of inactivation (mv) and activation (mv) properties of control ( $n_{\text{cells}}=12$ ) and HMW-AGEs ( $n_{\text{cells}}=8$ ) injected animals. Data are presented as mean  $\pm$  SEM. \* denotes  $p<0.05$

Parameters	Control	HMW-AGEs
Inactivation (mV)	$-29.6 \pm 0.5$	$-34.2 \pm 0.5$ *
Activation (mV)	$-18.7 \pm 0.5$	$-21.6 \pm 0.5$ *

**Fig. 5.** Morphometric analysis of cardiomyocyte organization reveals alterations with HMW-AGEs injections. (A) Toluidine blue-staining of LV cardiomyocytes from control (left panel) and HMW-AGEs (right panel) animals showing mitochondria (dark blue) and myofilaments/cytoplasm (light blue). (B) Quantification of mitochondrial surface area in cardiomyocytes from control ( $n_{\text{cells}}=90$ ) and HMW-AGEs ( $n_{\text{cells}}=165$ ) animals via thresholding. Mitochondrial surface area is expressed as a percentage of total cell area ( $p<0.0001$ , parametric unpaired t-test). (C) Representative electron micrographs of LV cardiomyocytes. Cardiomyocytes showed typical intracellular organization of myofilaments (light grey), mitochondria (dark grey) and cytoplasm (white). Magnification: 1800 $\times$ . Scale bars: 5  $\mu\text{m}$ . (D) Quantification of mitochondrial surface area, mitochondrial density, cytoplasm and myofilament surface area. Mitochondrial surface area in cardiomyocytes from control ( $n_{\text{cells}}=23$ ) and HMW-AGEs ( $n_{\text{cells}}=30$ ) animals ( $p=0.0471$ , parametric unpaired t-test). Intracellular fractions are expressed as a percentage of total grid points. Mitochondrial density calculated as the ratio of mitochondrial number to total cell area ( $p=0.0197$ , parametric unpaired t-test). Quantification of cytoplasm ( $p=0.0020$ , parametric unpaired t-test) and myofilament surface ( $p=0.1490$ , parametric unpaired t-test) areas in cardiomyocytes from control ( $n_{\text{cells}}=23$ ) and HMW-AGEs ( $n_{\text{cells}}=30$ ) animals. (E) Representative electron micrographs of the mitochondria in LV cardiomyocytes. Lower panels, enlargement of the marked area. Magnification: 14000 $\times$ . Scale bars: 2  $\mu\text{m}$ . Data are presented as mean  $\pm$  SEM. \* denotes  $p<0.05$ , \*\* denotes  $p<0.01$  and \*\*\*\*denotes  $p<0.0001$ .



Quantification of mitochondrial surface area, mitochondrial density, cytoplasm and myofilament surface area. Mitochondrial surface area in cardiomyocytes from control ( $n_{\text{cells}}=23$ ) and HMW-AGEs ( $n_{\text{cells}}=30$ ) animals ( $p=0.0471$ , parametric unpaired t-test). Intracellular fractions are expressed as a percentage of total grid points. Mitochondrial density calculated as the ratio of mitochondrial number to total cell area ( $p=0.0197$ , parametric unpaired t-test). Quantification of cytoplasm ( $p=0.0020$ , parametric unpaired t-test) and myofilament surface ( $p=0.1490$ , parametric unpaired t-test) areas in cardiomyocytes from control ( $n_{\text{cells}}=23$ ) and HMW-AGEs ( $n_{\text{cells}}=30$ ) animals. (E) Representative electron micrographs of the mitochondria in LV cardiomyocytes. Lower panels, enlargement of the marked area. Magnification: 14000 $\times$ . Scale bars: 2  $\mu\text{m}$ . Data are presented as mean  $\pm$  SEM. \* denotes  $p<0.05$ , \*\* denotes  $p<0.01$  and \*\*\*\*denotes  $p<0.0001$ .

cally significant difference between the groups, indicating no loss in myofilament content (Fig. 5D, fourth panel). In control animals, at a much higher magnification (14000x), mitochondria with intact cristae, nicely anchored to the sarcomeres were observed (Fig. 5E, left panel). After injection with HMW-AGEs, however and despite the presence of intact cristae, the attachment of the mitochondria to the sarcomeres was disrupted (Fig. 5E, right panel).

Finally, not only structure but also function of the mitochondria was altered. HMW-AGEs significantly decreased the activity of cytochrome c oxidase (COX) (Supplemental Fig. 4).

## Discussion

In this study, we showed that 6 weeks of HMW-AGEs injections lead to AGEs accumulation in the heart (Supplementary Fig. 5), resulting in cardiac dysfunction *in vivo*. This was the result of profound cardiomyocyte remodeling, including cell hypertrophy, reduced and slower fractional cell shortening, impaired myofilament properties associated with altered  $Ca^{2+}$ -influx and disturbed intracellular cardiomyocyte organization.

### *Physiological relevance of glycolaldehyde derived HMW-AGEs*

We injected healthy animals with HMW-AGEs prepared by incubating bovine serum albumin (BSA) with glycolaldehyde and concentrating the samples with a cut-off a 50 kDa. Glycolaldehyde, formed either as a fragmentation product in the Maillard reaction or as a result of the myeloperoxidase-hydrogen peroxide-chloride (MPO) reaction, can also react with proteins, resulting in AGEs formation [22]. The reaction between glycolaldehyde and amino acids has been shown to lead to the formation of specific AGEs such as CML and glycolaldehyde-pyridine (GA-pyridine) [23]. Several reports showed increased levels of these AGEs in diabetes patients and therefore indicating a role for modification of proteins with aldehydes in a diabetic setting [23-25]. Additionally, the presence of GA-pyridine has been found in human atherosclerotic fibrotic lesions and in glomerular mesangium in renal diseases, indicating their involvement in pathological situations [26, 27]. However, until now, no data have been available on the effect of glycolaldehyde-derived AGEs in the human heart *in vivo* as well as *in vitro*. Furthermore, Takeuchi *et al.* developed non-carboxymethyllysine anti-AGE antibodies that recognize serum proteins modified by short chain sugars or aldehydes (*e.g.* glyceraldehyde and glycolaldehyde) and dicarbonyl compounds (*e.g.* methylglyoxal and glyoxal). They show in their study that glycolaldehyde derived AGEs are present in serum from diabetic patients [28]. These results further confirm the physiological relevance of testing glycolaldehyde-derived AGEs. Finally, immunoblotting of serum protein samples from diabetic patients with glycolaldehyde-derived AGEs antibodies showed a high immunoreactivity around 200 kDa, indicating the presence of HMW glycolaldehyde-derived AGEs in diabetic patients [28]. However, to the best of our knowledge, the role of HMW-AGEs on cardiac function was until now not shown.

### *HMW-AGEs cause morphological remodeling and cardiomyocyte hypertrophy*

As shown previously, *in vivo* hypertrophy characterized by increased AWT and PWT has been observed in HMW-AGEs-treated animals [15]. The increase in heart mass was confirmed by the increase in HW/BW ratio and HW/TL ratio in our study. In addition, at the cellular level, cardiomyocytes subjected to chronic HMW-AGEs exposure were significantly wider. As also shown by others [29], our model displayed concentric hypertrophy, characterized by an increase in wall thickness and cardiac mass, with a small reduction in chamber volume. In addition, isolated cardiomyocytes are wider, indicating hypertrophy at the cellular level. Such LV cardiomyocyte remodeling has also been demonstrated by Gerdes *et al.* [30].

A potential trigger for the observed cardiomyocyte hypertrophy in our study could be the result of an increase in mechanical load which was evoked by the AGEs-induced cross-linking of extracellular matrix (ECM) components. The increase in tissue stiffness stimulates fibroblast differentiation, promoting collagen type I synthesis and cross-linking and the appearance of interstitial fibrosis. Evidence for this statement has been procured from a previous study by our research group in which an increase in interstitial fibrosis was reported in HMW-AGEs-treated rats [15]. This fibrosis will further enhance tissue stiffness thereby subjecting cardiomyocytes to a higher mechanical load [31]. In response to this maladaptive

remodeling process, an increase in angiotensin II (Ang II), endothelin 1 (ET-1) and insulin-like growth factor 1 (IGF1) concentration would activate intracellular signaling pathways leading to cell growth [32].

### *Impaired contractile properties are related to reduced $Ca^{2+}$ current and altered myofilament properties*

We observed no changes in cardiac output (CO) and ejection fraction (EF) *in vivo*. However, as already described previously [15], CO and EF are global parameters and are not sensitive enough to detect small changes. Nevertheless, at the cellular level a profound remodeling was observed, characterized by decreased unloaded shortening of intact cardiomyocytes associated with slower kinetics. The observed changes at the cellular level supported the *in vivo* data in which a statistically significant alteration of  $dP/dt_{max}$  was observed, indicating reduced ventricular contractility in rats treated with HMW-AGEs.

In our study, the reduced contraction was due to a reduced  $Ca^{2+}$  influx through L-type  $Ca^{2+}$  channels. Indeed, during ECC,  $Ca^{2+}$  is transported into the cytosol via L-type  $Ca^{2+}$  channels which are located in the transverse tubules (T-tubules). This  $Ca^{2+}$  influx through L-type  $Ca^{2+}$  channels cause  $Ca^{2+}$ -induced- $Ca^{2+}$ -release (CICR). High levels of  $Ca^{2+}$  are transported out of the SR into the cytosol to activate myofilaments and cause activation of the ECC resulting in cardiomyocyte contraction [33]. A reduced  $I_{CaL}$  will then result in reduced CICR and smaller contraction [34]. In our model as well as for other studies using diabetes models [35-38], cardiomyocytes isolated from treated animals displayed lower  $I_{CaL}$ , suggesting that the reduced  $Ca^{2+}$  influx could be a cause for the reduced contractile function. As the extent of the reduced contraction (-23.9%) corresponds to the extent of reduced  $I_{CaL}$  (-22%), it was likely that a change in the intrinsic properties of the L-type  $Ca^{2+}$  channel was the responsible underlying mechanism, rather than a decrease in protein density itself. In that context, we evaluated steady-state activation and inactivation of the L-type  $Ca^{2+}$  channel. Steady-state inactivation of the L-type  $Ca^{2+}$  channel, as a measure for channel availability, was significantly decreased in cells from HMW-AGEs animals indicating that the L-type  $Ca^{2+}$  channels were less available and inactivated more rapidly compared to cells from control animals. Therefore, less  $Ca^{2+}$  can be transported in the cytosol resulting in a reduced  $I_{CaL}$ . In line with our results, the L-type  $Ca^{2+}$  channel inactivation was also shown to be reduced in diabetes [39]. However, the exact underlying mechanism how HMW-AGEs induce these changed  $Ca^{2+}$ -channel properties remains unexplained. Whether the change in the L-type  $Ca^{2+}$  channel properties was mediated through RAGE activation was unlikely because we have shown in a previous study that HMW-AGEs did not act by RAGE activation [15].

In addition to reduced  $Ca^{2+}$  influx, impaired myofilament properties have been shown to be responsible for a reduced unloaded cell shortening [19, 40]. In our animal model, active force development tended to be reduced ( $P=0.06$ ). As also shown by others, a reduced CICR related to reduced  $Ca^{2+}$  influx is the primary cause for the impaired  $Ca^{2+}$  availability to bind on the myofilaments [19, 40]. Additionally, we observed a reduced rate of tension activation characterized by a significant decrease in maximal  $k_{tr}$ . A possible mechanism for the observed decrease could be a shift in myosin heavy chain (MHC) expression toward the slow  $\beta$ -isoform in the myofilaments of cardiomyocytes from HMW-AGEs-injected animals. However, we could not observe a shift in isoform expression between both groups (Supplementary Fig. 3). In addition, we observed an altered passive tension in response to HMW-AGEs. The decreased passive tension could due to an altered baseline sarcomere length or a greater intrinsic elasticity.

The PEVK segment of titin is able to bind actin which is important in the regulation of passive tension. Cardiomyocyte passive forces play an important role in cardiac muscle as it is part of the diastolic wall tension that determines the extent of filling of the heart [41]. Our data demonstrated a significantly decreased passive tension in skinned cardiomyocytes of HMW-AGEs animals. This was also observed in humans with chronic atrial fibrillation and patients with dilated cardiomyopathy (DCM) where the decreased passive tension is explained by a switch in titin isoforms [42, 43]. We could only speculate that a switch in titin

isoform plays a role in the observed decreased passive tension. However, literature shows that a reduced  $ICa_L$  can modify the interaction between titin and actin which in turn can contribute to decreased passive load [44], also observed in our model.

In diabetic animal models, it is widely shown that SERCA expression is decreased and PLN expression is increased causing arrhythmias and diabetic cardiomyopathy [45-47], while others failed to report these findings [48]. Petrova *et al.* reported that AGEs acutely have no effect on SERCA, PLN and NCX protein expression [49]. These data were in line with the results obtained in our experiments in a chronic setting. In our study, SERCA, PLN and their phosphorylated forms (T17 and S16) and NCX remained unchanged in animals treated with HMW-AGEs. Indeed, as shown by previous studies, an unchanged expression does not necessarily mean an unchanged protein activity that could, in addition to the altered ECC. In our study, the  $Ca^{2+}$  ATPase activity tended to decrease after injection of HMW-AGEs, possibly contributing to the impaired relaxation.

### *HMW-AGEs disrupt the cyto-architecture and functionality of cardiomyocytes*

The composition and organization of the cytoskeleton network are essential for cardiac cell function in adult cardiomyocytes. The number of myofilaments, the presence of a rigid cytoskeleton and a densely packed mitochondrial network contribute to normal cellular and architectural function. If these components are changed, contractile performance of cardiomyocytes will be altered. In our study, ultrastructural data showed no difference in myofilament content between both groups. However, a significant decrease in mitochondrial area and mitochondrial density indicated a disturbance in mitochondrial dynamics in cardiomyocytes of animals subjected to HMW-AGEs injections, leading to mitochondrial damage. Literature has shown that AGEs can disrupt mitochondrial network dynamics leading to damage of the mitochondria [50, 51]. In addition, AGEs could stimulate their degradation by mitophagy by activating PI3K/AKT/mTOR and ERK signaling pathways [52, 53]. Additionally, Viola *et al.* described that changes in  $Ca^{2+}$ -influx as well as changes in L-type  $Ca^{2+}$  channel activity were sufficient to modulate mitochondrial function via an association through the cytoskeleton. It is then likely that HMW-AGEs could indirectly modify mitochondrial function by altering L-type  $Ca^{2+}$  channel properties. Furthermore, we observed a significant increased cytoplasm fraction in the HMW-AGEs group compared to control. More cytoplasm density results in more space between the myofilaments, leading to an altered cell architecture which is essential for proper cardiomyocyte contractile function. Our data demonstrated that HMW-AGEs disrupt the cyto-architecture of cardiomyocytes through disorganization of the mitochondrial network.

In addition, to explore the functional consequences related to the structural alterations of the mitochondria, we determined the activity of COX. COX is the terminal complex (complex IV) of the electron transfer chain. It catalyzes the transfer of electrons from ferrocytochrome c to oxygen, converting the latter to water. Alterations in the activity of COX has been associated with mitochondrial defects. Li *et al.* reported that dysfunctional cytochrome c oxidase leads to a compromised mitochondrial membrane potential and a decreased ATP level [54]. As shown in Supplementary Fig. 4, COX activity was significantly reduced with HMW-AGEs, resulting in a decreased mitochondrial functionality. These results were in line with data regarding the decreased  $Ca^{2+}$  ATPase activity.

## Conclusion

The currently investigated anti-AGEs therapies are unconvincing as they only target LMW-AGEs. Our data indicate that HMW-AGEs also impair cardiomyocyte structure and function via a different working mechanism from LMW-AGEs, indicating that HMW-AGEs play a distinct role in the development of cardiac dysfunction. In the future, targeting the deleterious effects of HMW-AGEs, could be a new strategy to improve cardiac outcome in cardiovascular diseases.

## Abbreviations

AGEs (Advanced glycation end-products); Ang II (Angiotensin II); AWT (Anterior wall thickness); BES (N,N-Bis(2-hydroxyethyl)-2-aminoethanesulfonic acid); BSA (Bovine serum albumin); CICR (Ca<sup>2+</sup>-induced-Ca<sup>2+</sup>-release); CO (Cardiac output); COX (Cytochrome c oxidase); CVD (Cardiovascular diseases); DCM (Dilated cardiomyopathy);  $dP/dt_{max}$  (Maximum peak time derivative);  $dP/dt_{min}$  (Minimum peak time derivative); ECM (Extracellular matrix); EF (Ejection fraction); EM (Electron microscopic); ET-1 (Endothelin 1);  $F_{act}$  (Active tension);  $F_{pass}$  (Passive force); G (Conductance); HF (Heart failure); HMW-AGEs (High-molecular-weight AGEs); HR (Heart rate); HW/BW (Heart weight/body weight); HW/TL (Heart weight/tibia length); I (Current);  $I_{CaL}$  (L-type Ca<sup>2+</sup> current); IGF1 (Insulin-like growth factor 1); i.p. (Intraperitoneally); ISO (Isoproterenol);  $K_{tr}$  (Rate of force redevelopment);  $L/L_0$  (Unloaded cell shortening normalized to diastolic cell length); LM (Light microscopic); LMW-AGEs (Low-molecular-weight AGEs); LV (Left ventricular); MHC- $\alpha/\beta$  (Myosin heavy chain-alpha/beta); NT (Normal Tyrode); PWT (Posterior wall thickness);  $RT_{50}$  (Time to half-maximal relaxation); SERCA (Sarco/endoplasmic reticulum Ca<sup>2+</sup> ATPase); SEM (Standard error of the mean); Tau (Time constant for isovolumetric relaxation); TTP (Time to peak contraction); T-tubules (Transverse tubules);  $V_{50}$  (Voltage value at 50% inactivation);  $\tau_{slow}$  (Slow inactivation component of Ca<sup>2+</sup> current).

## Acknowledgements

We thank Marc Jans for assisting with the EM. The authors also thank Petra Bex, Rosette Beenaerts and Kanigula Mubagwa for their skillful technical assistance. The graphical abstract was created using images from Servier Medical Art Commons Attribution 3.0 Unported License (<http://smart.servier.com>). Servier Medical Art by Servier is licensed under a Creative Commons Attribution 3.0 Unported License.

## Author Contributions

DD and LE generated the original idea and hypothesis, designed the experiments and wrote the manuscript. DD, LE, SH, RD, DK, MV and HB performed the experiments and conducted data analysis. SH, RD, DK, MV, HB, JV and IL provided valuable feedback and helped revise the draft. VB provided the headship for the project and furnished valuable feedback for revising the draft.

## Funding

This work was supported by a Bijzonder onderzoeksfonds (BOF) grant from Hasselt University (15NI06-BOF).

## Statement of Ethics

The animal protocol was approved by the Local Ethical Committee (Ethical Commission for Animal Experimentation, UHasselt, Diepenbeek, Belgium). All animal procedures were performed conforming to the guidelines from Directive 2010/63/EU of the European Parliament on the protection of animals used for scientific purposes. Only trained researchers, certified with a Laboratory Animal Science course according to the Federation of European Laboratory Animal Science Associations, performed animal handling and procedures.

## Disclosure Statement

The authors have no conflicts of interest to declare.

## References

- 1 UN. United Nations population division: Population aged 65 or over 2012. <http://data.un.org/Data.aspx?q=worldpopulation+over+65&d=PopDiv&f=variableID%3a23%3bcrID%3a900>
- 2 Braunwald E: Research advances in heart failure: a compendium. *Circ Res* 2013;113:633-645.
- 3 Verboven M, Deluyker D, Ferferieva V, Lambrichts I, Hansen D, Eijnde BO, Bito V: Western diet given to healthy rats mimics the human phenotype of diabetic cardiomyopathy. *J Nutr Biochem* 2018;61:140-146.
- 4 Shah MS, Brownlee M: Molecular and Cellular Mechanisms of Cardiovascular Disorders in Diabetes. *Circ Res* 2016;118:1808-1829.
- 5 Acharya AS, Manning JM: Reaction of glycolaldehyde with proteins: latent crosslinking potential of alpha-hydroxyaldehydes. *Proc Natl Acad Sci U S A* 1983;80:3590-3594.
- 6 Singh R, Barden A, Mori T, Beilin L: Advanced glycation end-products: a review. *Diabetologia* 2001;44:129-146.
- 7 Hartog JW, Voors AA, Bakker SJ, Smit AJ, van Veldhuisen DJ: Advanced glycation end-products (AGEs) and heart failure: pathophysiology and clinical implications. *Eur J Heart Fail* 2007;9:1146-1155.
- 8 Hegab Z, Gibbons S, Neyses L, Mamas MA: Role of advanced glycation end products in cardiovascular disease. *World J Cardiol* 2012;4:90-102.
- 9 Gerdemann A, Lemke HD, Nothdurft A, Heidland A, Munch G, Bahner U, Schinzel R: Low-molecular but not high-molecular advanced glycation end products (AGEs) are removed by high-flux dialysis. *Clin Nephrol* 2000;54:276-283.
- 10 Grzebyk E, Knapik-Kordecka M, Piwowar A: Advanced glycation end-products and cathepsin cysteine protease in type 2 diabetic patients. *Pol Arch Med Wewn* 2013;123:364-370.
- 11 Koyama H, Yamamoto H, Nishizawa Y: RAGE and soluble RAGE: potential therapeutic targets for cardiovascular diseases. *Mol Med* 2007;13:625-635.
- 12 Willemsen S, Hartog JW, van Veldhuisen DJ, van der Meer P, Roze JF, Jaarsma T, Schalkwijk C, van der Horst IC, Hillege HL, Voors AA: The role of advanced glycation end-products and their receptor on outcome in heart failure patients with preserved and reduced ejection fraction. *Am Heart J* 2012;164:742-749 e743.
- 13 Deluyker D, Evens L, Bito V: Advanced glycation end products (AGEs) and cardiovascular dysfunction: focus on high molecular weight AGEs. *Amino Acids* 2017;49:1535-1541.
- 14 Deluyker D, Evens L, Belien H, Bito V: Acute exposure to glycated proteins reduces cardiomyocyte contractile capacity. *Exp Physiol* 2019;104:997-1003.
- 15 Deluyker D, Ferferieva V, Noben JP, Swennen Q, Bronckaers A, Lambrichts I, Rigo JM, Bito V: Cross-linking versus RAGE: How do high molecular weight advanced glycation products induce cardiac dysfunction? *Int J Cardiol* 2016;210:100-108.
- 16 Deluyker D, Ferferieva V, Driesen RB, Verboven M, Lambrichts I, Bito V: Pyridoxamine improves survival and limits cardiac dysfunction after MI. *Sci Rep* 2017;7:16010.
- 17 Bito V, Macquaide N, Sipido KR: Characterizing the trigger for sarcoplasmic reticulum Ca<sup>2+</sup> release in cardiac myocytes. *Cold Spring Harb Protoc* 2015;2015:398-402.
- 18 Vornanen M: Na<sup>+</sup>/Ca<sup>2+</sup> exchange current in ventricular myocytes of fish heart: contribution to sarcolemmal Ca<sup>2+</sup> influx. *J Exp Biol* 1999;202:1763-1775.
- 19 Bito V, van der Velden J, Claus P, Dommke C, Van Lommel A, Mortelmans L, Verbeken E, Bijmens B, Stienen G, Sipido KR: Reduced force generating capacity in myocytes from chronically ischemic, hibernating myocardium. *Circ Res* 2007;100:229-237.
- 20 Bollen IAE, Ehler E, Fleischanderl K, Bouwman F, Kempers L, Ricke-Hoch M, Hilfiker-Kleiner D, Dos Remedios CG, Kruger M, Vink A, Asselbergs FW, van Spaendonck-Zwarts KY, Pinto YM, Kuster DWD, van der Velden J: Myofilament Remodeling and Function Is More Impaired in Peripartum Cardiomyopathy Compared with Dilated Cardiomyopathy and Ischemic Heart Disease. *Am J Pathol* 2017;187:2645-2658.
- 21 Schindelin J, Arganda-Carreras I, Frise E, Kaynig V, Longair M, Pietzsch T, Preibisch S, Rueden C, Saalfeld S, Schmid B, Tinevez JY, White DJ, Hartenstein V, Eliceiri K, Tomancak P, Cardona A: Fiji: an open-source platform for biological-image analysis. *Nat Methods* 2012;9:676-682.
- 22 Anderson MM, Hazen SL, Hsu FF, Heinecke JW: Human neutrophils employ the myeloperoxidase-hydrogen peroxide-chloride system to convert hydroxy-amino acids into glycolaldehyde, 2-hydroxypropanal, and acrolein. A mechanism for the generation of highly reactive alpha-hydroxy and alpha,beta-unsaturated aldehydes by phagocytes at sites of inflammation. *J Clin Invest* 1997;99:424-432.

- 23 Mera K, Takeo K, Izumi M, Maruyama T, Nagai R, Otagiri M: Effect of reactive-aldehydes on the modification and dysfunction of human serum albumin. *J Pharm Sci* 2010;99:1614-1625.
- 24 Atkins TW, Thornally PJ: Erythrocyte glyoxalase activity in genetically obese (ob/ob) and streptozotocin diabetic mice. *Diabetes Res* 1989;11:125-129.
- 25 Odani H, Shinzato T, Matsumoto Y, Usami J, Maeda K: Increase in three alpha,beta-dicarbonyl compound levels in human uremic plasma: specific *in vivo* determination of intermediates in advanced Maillard reaction. *Biochem Biophys Res Commun* 1999;256:89-93.
- 26 Greven WL, Waanders F, Nagai R, van den Heuvel MC, Navis G, van Goor H: Mesangial accumulation of GA-pyridine, a novel glycolaldehyde-derived AGE, in human renal disease. *Kidney Int* 2005;68:595-602.
- 27 Nagai R, Hayashi CM, Xia L, Takeya M, Horiuchi S: Identification in human atherosclerotic lesions of GA-pyridine, a novel structure derived from glycolaldehyde-modified proteins. *J Biol Chem* 2002;277:48905-48912.
- 28 Takeuchi M, Makita Z, Bucala R, Suzuki T, Koike T, Kameda Y: Immunological evidence that non-carboxy-methyllysine advanced glycation end-products are produced from short chain sugars and dicarbonyl compounds *in vivo*. *Mol Med* 2000;6:114-125.
- 29 Grossman W, Jones D, McLaurin LP: Wall stress and patterns of hypertrophy in the human left ventricle. *J Clin Invest* 1975;56:56-64.
- 30 Gerdes AM: Cardiac myocyte remodeling in hypertrophy and progression to failure. *J Card Fail* 2002;8:S264-268.
- 31 Candido R, Forbes JM, Thomas MC, Thallas V, Dean RG, Burns WC, Tikellis C, Ritchie RH, Twigg SM, Cooper ME, Burrell LM: A breaker of advanced glycation end products attenuates diabetes-induced myocardial structural changes. *Circ Res* 2003;92:785-792.
- 32 Bernardo BC, Weeks KL, Pretorius L, McMullen JR: Molecular distinction between physiological and pathological cardiac hypertrophy: experimental findings and therapeutic strategies. *Pharmacol Ther* 2010;128:191-227.
- 33 Bers DM: Cardiac excitation-contraction coupling. *Nature* 2002;415:198-205.
- 34 Piacentino V 3rd, Weber CR, Chen X, Weisser-Thomas J, Margulies KB, Bers DM, Houser SR: Cellular basis of abnormal calcium transients of failing human ventricular myocytes. *Circ Res* 2003;92:651-658.
- 35 Bracken N, Howarth FC, Singh J: Effects of streptozotocin-induced diabetes on contraction and calcium transport in rat ventricular cardiomyocytes. *Ann N Y Acad Sci* 2006;1084:208-222.
- 36 Bracken NK, Woodall AJ, Howarth FC, Singh J: Voltage-dependence of contraction in streptozotocin-induced diabetic myocytes. *Mol Cell Biochem* 2004;261:235-243.
- 37 Lu Z, Ballou LM, Jiang YP, Cohen IS, Lin RZ: Restoration of defective L-type Ca<sup>2+</sup> current in cardiac myocytes of type 2 diabetic db/db mice by Akt and PKC- $\iota$ . *J Cardiovasc Pharmacol* 2011;58:439-445.
- 38 Pereira L, Matthes J, Schuster I, Valdivia HH, Herzig S, Richard S, Gomez AM: Mechanisms of [Ca<sup>2+</sup>]<sub>i</sub> transient decrease in cardiomyopathy of db/db type 2 diabetic mice. *Diabetes* 2006;55:608-615.
- 39 Yuill KH, Al Kury LT, Howarth FC: Characterization of L-type calcium channel activity in atrioventricular nodal myocytes from rats with streptozotocin-induced Diabetes mellitus. *Physiol Rep* 2015;3:e12632.
- 40 Bito V, Heinzl FR, Weidemann F, Dommke C, van der Velden J, Verbeken E, Claus P, Bijmens B, De Scheerder I, Stienen GJ, Sutherland GR, Sipido KR: Cellular mechanisms of contractile dysfunction in hibernating myocardium. *Circ Res* 2004;94:794-801.
- 41 Allen DG, Kentish JC: The cellular basis of the length-tension relation in cardiac muscle. *J Mol Cell Cardiol* 1985;17:821-840.
- 42 Belus A, Piroddi N, Ferrantini C, Tesi C, Cazorla O, Toniolo L, Drost M, Mearini G, Carrier L, Rossi A, Mugelli A, Cerbai E, van der Velden J, Poggesi C: Effects of chronic atrial fibrillation on active and passive force generation in human atrial myofibrils. *Circ Res* 2010;107:144-152.
- 43 Makarenko I, Opitz CA, Leake MC, Neagoe C, Kulke M, Gwathmey JK, del Monte F, Hajjar RJ, Linke WA: Passive stiffness changes caused by upregulation of compliant titin isoforms in human dilated cardiomyopathy hearts. *Circ Res* 2004;95:708-716.
- 44 Viola HM, Hool LC: Role of the cytoskeleton in communication between L-type Ca<sup>2+</sup> channels and mitochondria. *Clin Exp Pharmacol Physiol* 2013;40:295-304.
- 45 Zarain-Herzberg A, Garcia-Rivas G, Estrada-Aviles R: Regulation of SERCA pumps expression in diabetes. *Cell Calcium* 2014;56:302-310.

- 46 Zhao XY, Hu SJ, Li J, Mou Y, Chen BP, Xia Q: Decreased cardiac sarcoplasmic reticulum Ca<sup>2+</sup>-ATPase activity contributes to cardiac dysfunction in streptozotocin-induced diabetic rats. *J Physiol Biochem* 2006;62:1-8.
- 47 Kim HW, Ch YS, Lee HR, Park SY, Kim YH: Diabetic alterations in cardiac sarcoplasmic reticulum Ca<sup>2+</sup>-ATPase and phospholamban protein expression. *Life Sci* 2001;70:367-379.
- 48 Teshima Y, Takahashi N, Saikawa T, Hara M, Yasunaga S, Hidaka S, Sakata T: Diminished expression of sarcoplasmic reticulum Ca(2+)-ATPase and ryanodine sensitive Ca(2+)Channel mRNA in streptozotocin-induced diabetic rat heart. *J Mol Cell Cardiol* 2000;32:655-664.
- 49 Petrova R, Yamamoto Y, Muraki K, Yonekura H, Sakurai S, Watanabe T, Li H, Takeuchi M, Makita Z, Kato I, Takasawa S, Okamoto H, Imaizumi Y, Yamamoto H: Advanced glycation endproduct-induced calcium handling impairment in mouse cardiac myocytes. *J Mol Cell Cardiol* 2002;34:1425-1431.
- 50 Dorn GW, 2nd: Mitochondrial dynamism and heart disease: changing shape and shaping change. *EMBO Mol Med* 2015;7:865-877.
- 51 Neviere R, Yu Y, Wang L, Tessier F, Boulanger E: Implication of advanced glycation end products (Ages) and their receptor (Rage) on myocardial contractile and mitochondrial functions. *Glycoconj J* 2016;33:607-617.
- 52 Hou X, Hu Z, Xu H, Xu J, Zhang S, Zhong Y, He X, Wang N: Advanced glycation endproducts trigger autophagy in cardiomyocyte via RAGE/PI3K/AKT/mTOR pathway. *Cardiovasc Diabetol* 2014;13:78.
- 53 Hu P, Zhou H, Lu M, Dou L, Bo G, Wu J, Huang S: Autophagy Plays a Protective Role in Advanced Glycation End Product-Induced Apoptosis in Cardiomyocytes. *Cell Physiol Biochem* 2015;37:697-706.
- 54 Li Y, Park JS, Deng JH, Bai Y: Cytochrome c oxidase subunit IV is essential for assembly and respiratory function of the enzyme complex. *J Bioenerg Biomembr* 2006;38:283-291.